International Journal of Medical, Medicine and Health Sciences
ISSN: 2517-9969
Vol:9, No:8, 2015

Identification of High Stress and Strain Regions in Proximal Femur during Single-Leg Stance and Sideways Fall Using QCT-Based Finite Element Model

H. Kheirollahi, Y. Luo

***Abstract*—**Studying stress and strain trends in the femur and recognizing femur failure mechanism is very important for preventing hip fracture in the elderly. The aim of this study was to identify high stress and strain regions in the femur during normal walking and falling to find the mechanical behavior and failure mechanism of the femur. We developed a finite element model of the femur from the subject's quantitative computed tomography (QCT) image and used it to identify potentially high stress and strain regions during the single-leg stance and the sideways fall. It was found that fracture may initiate from the superior region of femoral neck and propagate to the inferior region during a high impact force such as sideways fall. The results of this study showed that the femur bone is more sensitive to strain than stress which indicates the effect of strain, in addition to effect of stress, should be considered for failure analysis.

***Keywords*—**Finite element analysis, hip fracture, strain, stress.

I. Introduction

THE femur is one of the long bones in the human body. For the elderly, especially for those who have osteoporosis, the femur is prone to facture during walking and falling. Hip fracture is increasing annually and leads to social problems for the elderly. It is associated with an up to 20% chance of death, a 25% chance of long term disability and less than a 50% chance of full recovery [1]. The devastating squeal of hip fracture in individual's long-term life have motivated us to identify high stress and strain regions in the femur during walking and falling to provide an appropriate plan to prevent hip fracture in the elderly.

The stress and strain distributions in the femur is affected by a number of factors, for example, the subject's height and weight, the size of femur, and the bone mineral density (BMD). All these factors are subject-dependent. Therefore, a subject-specific finite element model is more accurate to predict femur stresses and strains. High stress and strain regions in the femur are the potential locations of developing cracks and then leading to hip fracture. By finding the high stress and strain regions of the femur during normal walking and falling, its mechanical behavior and failure mechanism can be recognized. Dual-energy x-ray absorptiometry (DXA)- and quantitative computed tomography (QCT)-based finite element (FE) modeling are two non-invasive methods for in-vivo assessment of the human femur under the loading conditions. Whereas DXA-based FE models are two-dimensional (2-D) and are not able to represent the real-world case; a QCT-based FE model, which is three-dimensional (3-D), is preferred.

Several reported studies used QCT-based finite models to predict potential fracture location, bone strength, fracture load, and stress/strain distribution [2]-[6]. Although there were exceptions, clinical observations have revealed that the majority of hip fractures occurred at either the smallest femoral neck, or the intertrochanteric, or the sub trochanteric cross-section [7]. Therefore, in our study, the objective is to develop a FE model of femur from the subject's QCT image to identify the stress and strain trends at the three critical cross-sections.

II. Materials and Methods

In this section the methodology to construct the QCT-based FE model and analysis of femur under the loading and boundary conditions is described.

A. QCT-Scan of Femur

The 3-D model of the femur can be constructed from the subject's femur QCT image. QCT slices are produced using multiple scanners with a set of proper acquisition and reconstruction parameters (Fig. 1 (a)). Slice thickness of 1mm is commonly used. The scanned QCT images are stored in the format of Digital Imaging and Communications in Medicine (DICOM), which can be used for the construction of a 3-D FE model. A proper segmentation is done to separate the femur for constructing the 3-D model. Each voxel in the QCT scan has an intensity (or grey scale) that is expressed as Hounsfield Unit (HU), which is correlated to bone density [8], [9]. QCT images of 10 clinical cases (5 females and 5 males), totally 20 right and left femurs, were acquired from the Winnipeg Health Science Centre in an anonymous way under a human research ethics approval. The subjects are in the age scope from 50 to 74 years (average 64.4 years).

B. Construction of Finite Element Model

In the first step, the geometrical model of the femur is generated from clinical QCT images using Mimics (Materialize, Leuven, Belgium). QCT images (in DICOM

Hossein Kheirollahi is with the Department of Mechanical Engineering, University of Manitoba, Winnipeg, MB, Canada (e-mail: kheirolh@myumanitoba.ca).

Yunua Luo is with the Department of Mechanical Engineering, University of Manitoba, Winnipeg, MB, Canada and the Department of Anatomy, Southern Medical University, Guangzhou, China (e-mail: Yunhua.Luo@umanitoba.ca).

format) are imported to Mimics for segmentation (Fig. 1 (a)) and construction of 3-D geometric model of the femur (Fig. 1 (b)). With the 3-D geometric model, a FE mesh is generated using the 3-matic module in Mimics (Fig. 1 (c)). The 4-node linear tetrahedral element SOLID72 in ANSYS was used in this study. To investigate model convergence, FE models with different maximum element edge lengths were created. For each FE model, displacement was calculated under the same loading and boundary conditions. The maximum element edge length that produced converged finite element solutions was obtained and used in all the rest FE simulations.

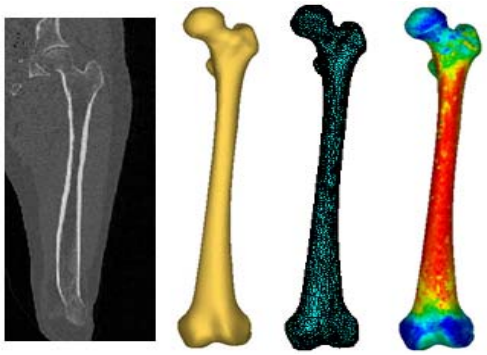

(a) (b) (c) (d)

Fig. 1 Construction of subject-specific QCT-based finite element model: (a) QCT-scan of the subject's femur; (b) 3-D geometric model generated from the QCT scans; (c) 3-D finite element model; and (d) inhomogeneous material properties distribution

C. Assignment of Material Properties

To construct a faithful FE model, bone material properties are considered inhomogeneous and isotropic in this study. Information on the inhomogeneous isotropic mechanical properties of the bone can be derived from the CT data using a mathematical relationship between the CT numbers and the mechanical properties of bone. The following empirical equation was used to determine bone ash density (ρ_{ash}) according to the HU number [5], [10]:

$$\rho_{ash} = 0.04162 + 0.000854\,HU \quad (g/cm^3) \tag{1}$$

Equations (2) and (3), derived by Keller [11], were respectively used to assign Young's modulus (E) and the yield stress (σ_Y) according to the bone ash density:

$$E = 10500\rho_{ash}^{2.29} \quad (MPa) \tag{2}$$

$$\sigma_Y = 116\rho_{ash}^{2.03} \quad (MPa) \tag{3}$$

A constant Poisson's ratio ($\nu = 0.4$) was considered [12]-[14]. To assign material properties, elements are grouped into several discrete material bins using Mimics (Materialize, Leuven, Belgium), which are used to approximately represent the continuous distribution of the inhomogeneous bone mechanical properties. To determine the maximum number of material bins, convergence study was performed. Models with different material bins were created for convergence study. For each FE model, displacement was calculated under the same loading and boundary conditions. The maximum number of material bins that generated converged finite element solutions was obtained. Fig. 1 (d) shows the isotropic inhomogeneous distribution of material properties.

D. Finite Element Analysis Using ANSYS

A finite element model of femur with the assigned material properties output from Mimics was imported to ANSYS for finite element analysis. For a precise assessment of hip fracture risk during the single-leg stance and the sideways fall, loading and boundary conditions simulating the single-leg stance and the sideways fall configurations are required in the FE model. To simulate the single-leg stance statue, 2.5 times of the patient's body weight was applied as a distributed load on the femoral head [15] and femur was fixed at the distal end [12], [16] (see Fig. 2 (a)):

$$F_{Stance} = 2.5w \quad (N) \tag{4}$$

where w is the subject's body weight in Newton (N). To simulate sideways fall configuration, the distal end of femur were completely fixed and the surface of femoral head were fixed in the loading direction (Fig. 2 (b)) [6], [17]. The impact force during the sideways fall acting on the greater trochanter (Fig. 2 (b)) is given by [15], [18]:

$$F_{Impact} = 8.25w\left(\frac{h}{170}\right)^{\frac{1}{2}} \quad (N) \tag{5}$$

where h is the height of the subject in centimeter (cm). Loading and boundary conditions on the greater trochanter, the femoral head, and the distal end of femur were applied to a group of nodes using ANSYS Parametric Design Language (APDL) codes (Figs. 2 (a) and (b)). After importing the QCT-based FE model and applying the loading and boundary conditions, finite element analysis was performed and finite element solutions were obtained. In all the analysis, stresses and strains were obtained for each subject.

A. Detection of the Three Critical Cross-Sections on the Femur

Hip fractures usually are categorized into three major types based on the anatomical locations: femoral neck, intertrochanteric, and sub trochanteric fracture (Fig. 3). According to clinical observations, 49 percent of hip fractures are intertrochanteric, 37 percent are at femoral neck, and 14 percent are sub trochanteric [7]. Therefore, the smallest femoral neck cross-section (SFN CS), the intertrochanteric cross-section (IntT CS), and the sub trochanteric cross-section (SubT CS) are three critical cross-sections of femur that usually have the highest fracture risk (Fig. 3). To determine the smallest femoral neck cross-section and the intertrochanteric cross-section, neck-shaft angle is needed. The neck-shaft angle is the angle between the femoral neck axis and the femoral shaft axis. This angle traditionally is measured on conventional radiography images, or using 2-D

images projected from CT/MRI data. In spite of their popularity, these methods are based on over simplification of the real 3-D anatomy and may lead to large errors due to the inaccuracy in selection of the measurement plane [19]-[21]. In this study, the neck-shaft angle was measured using a 3-D measurement technique based on fitting functions. In this technique, the shapes of particular parts of the femur are approximated using geometric entities such as circle, cylinder, sphere, and etc., which are well-fitted to the actual anatomy, and the geometrical relationships between these entities are obtained to estimate the neck-shaft angle.

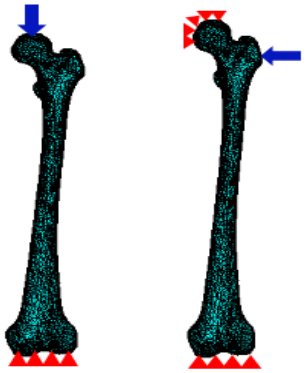

(a) (b)

Fig. 2 Application of loading and boundary conditions during (a) the single-leg stance, and (b) the sideways fall

With the femoral neck-shaft angle, the intertrochanteric cross-section and the smallest femoral neck cross-section were found using in-house computer codes. The smallest femoral neck cross-section has the smallest area in the neck region and the intertrochanteric cross-section has the largest area in the intertrochanteric region [22]. The sub trochanteric cross-section is located five centimeter below the lesser trochanter [23] (Fig. 3).

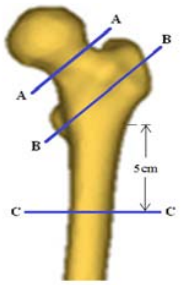

Fig. 3 Three critical cross-sections of femur: the smallest femoral neck cross-section (A-A), the intertrochanteric cross-section (B-B), and the sub trochanteric cross-section (C-C)

III. Results

A. Convergence Study

The convergence of finite element solutions is usually achieved by refining the finite element mesh with the same loading and boundary conditions. The displacement at a predefined point is monitored to judge if a convergence has been achieved, or not. The results of the convergence study showed that the displacements did not change significantly for the FE models with the maximum element edge length lower than 8 mm, meaning that a convergence was achieved with the above maximum element edge length. Therefore, in the construction of all femur FE models, the maximum element edge length was set to 8mm.

For convergence study in assigning the inhomogeneous material properties, 3-D femur FE models with different material bins were created. For each FE model with different material bins, the maximum displacement at the smallest femoral neck cross-section was monitored under the same loading and boundary conditions. The displacements were compared among the FE models with different material bins. The results of the convergence study showed that the displacement did not change significantly in the FE models with the number of material bins higher than 50. Therefore, in the assignment of femur inhomogeneous material properties, 50 discrete material bins were considered.

B. Stress and strain Distributions at the Three Critical Cross-Sections

The results of the finite element analyses showed that during the single-leg stance, the tensile stress (σ_1) in the superior region of the femoral neck is higher than that in the inferior region (Figs. 4 (a) and 6 (a)); and the compressive stress (σ_3) in the inferior region is higher than that in the superior region (Figs. 4 (b) and 6 (b)). Conversely, during the sideways fall, the tensile stress in the inferior region of femoral neck is higher than that in the superior region (Figs. 5 (a) and 7 (a)) and the compressive stress in the superior region is higher than that in the inferior region (Figs. 5 (b) and 7 (b)). During the single-leg stance; the maximum tensile stress, occurring at the superior femoral neck, is lower than the maximum compressive stress, occurring at the inferior femoral neck; while during the sideways fall, the maximum compressive stress, occurring at the superior femoral neck, is larger than maximum tensile stress, occurring at the inferior femoral neck (Table I).

For the 10 clinical cases (5 females and 5 males, totally 20 right and left femurs), the maximum von Mises stress and strain at the three critical cross-sections of femur during both the single-leg stance and the sideways fall were calculated and the results are respectively shown in Figs. 8 and 9. It was observed that during the sideways fall, the femoral neck and the intertrochanteric region experience higher stresses than the sub trochanteric region (Table III); but during the single-leg stance, there is not very much difference between the stresses in the three regions (Table II); for some cases, the stresses at the sub trochanteric region are in the same range as (or even higher than) the stresses at the femoral neck and the intertrochanteric region during the single-leg stance (Fig. 8). Strains at the femoral neck and the intertrochanteric region are also much higher than those at the sub trochanteric region during both the single-leg stance and the sideways fall (Tables IV and V).

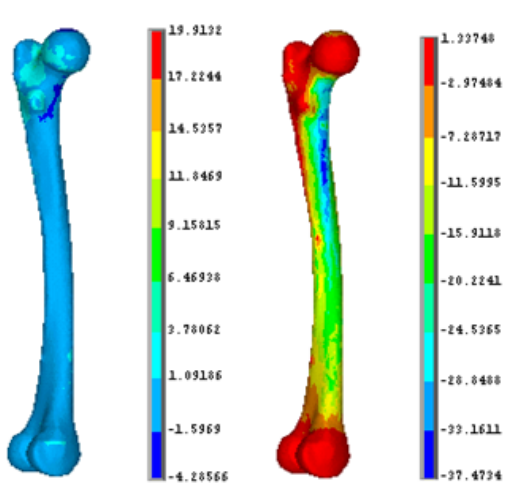

(a) (b)

Fig. 4 (a) The tensile stress (MPa) and (b) the compressive stress (MPa) distributions in the femur during the single-leg stance

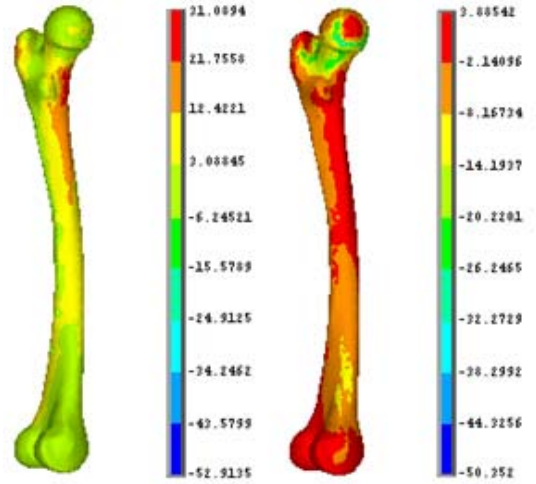

(a) (b)

Fig. 5 (a) The tensile stress (MPa) and (b) the compressive stress (MPa) distributions in the femur during the sideways fall

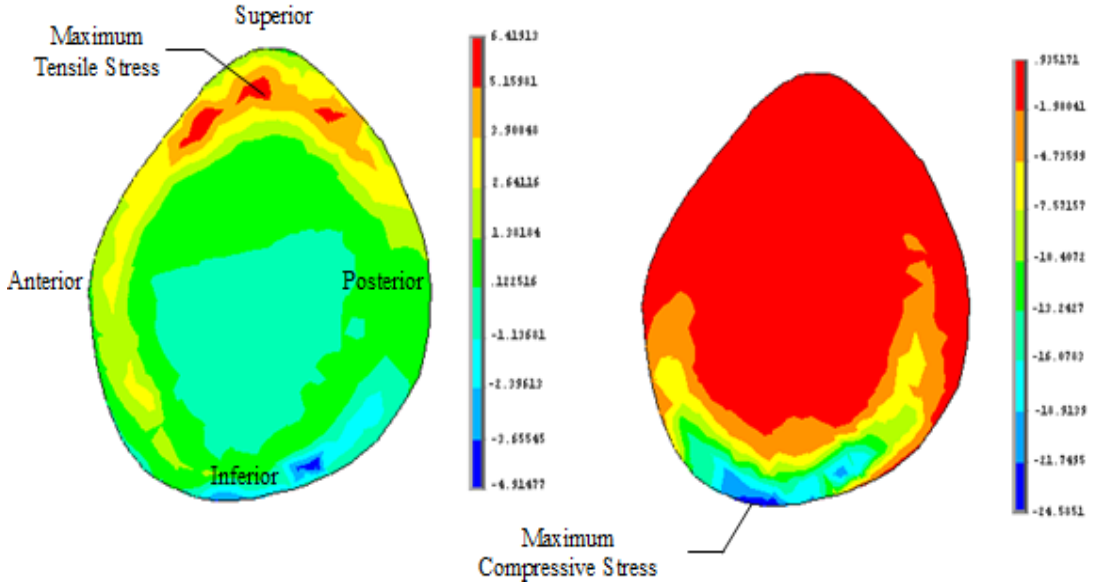

(a) (b)

Fig. 6 (a) The tensile stress (MPa) and (b) the compressive stress (MPa) distributions at the smallest femoral neck cross-section during the single-leg stance

TABLE I
COMPARISON OF TENSILE STRESS AND COMPRESSIVE STRESS DISTRIBUTIONS IN THE FEMORAL NECK OF A CLINICAL CASE DURING THE SINGLE-LEG STANCE AND THE SIDEWAYS FALL

	Single-Leg Stance		Sideways Fall	
	Maximum Tensile Stress (MPa)	Maximum Compressive Stress (MPa)	Maximum Tensile Stress (MPa)	Maximum Compressive Stress (MPa)
	6.41	24.58	10.11	29.66
Corresponding occurring region	Superior femoral neck	Inferior femoral neck	Inferior femoral neck	Superior femoral neck

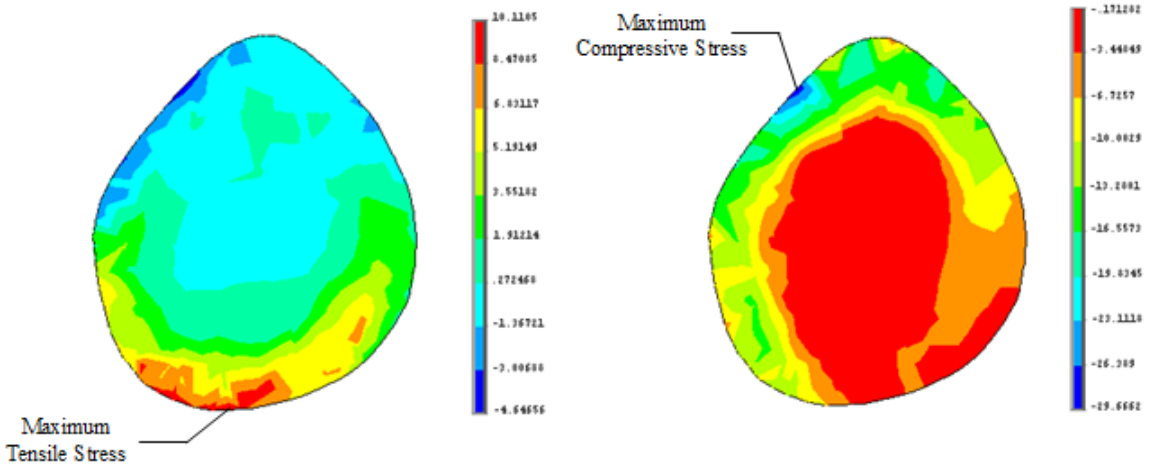

(a) (b)

Fig. 7 (a) The tensile stress (MPa), and (b) the compressive stress (MPa) distributions at the smallest femoral neck cross-section during the sideways fall

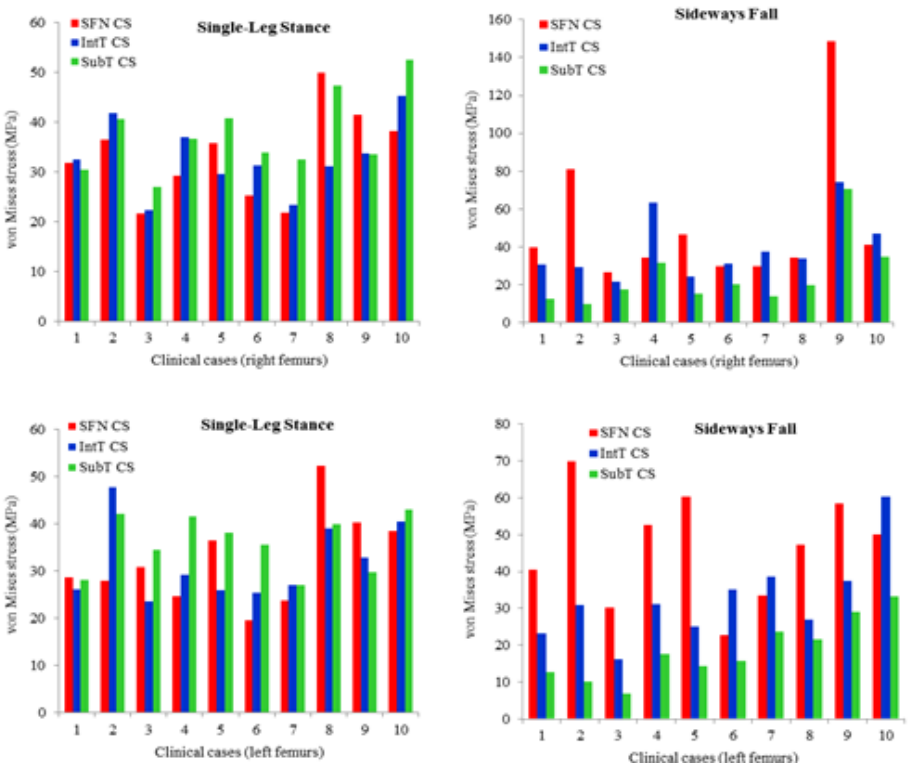

Fig. 8 The maximum von Mises stress (MPa) at the smallest femoral neck cross-section (SFN CS), the intertrochanteric cross-section (IntT CS), and the subtrochanteric cross-section (SubT CS) of right and left femurs of 10 clinical cases during the single-leg stance and the sideways fall

TABLE II
AVERAGE MAXIMUM VON MISES STRESS (MPA) AT THE SMALLEST FEMORAL NECK CROSS-SECTION (SFN CS), THE INTERTROCHANTERIC CROSS-SECTION (INTT CS), AND THE SUBTROCHANTERIC CROSS-SECTION (SUBT CS) OF RIGHT AND LEFT FEMURS OF 10 CLINICAL CASES DURING THE SINGLE-LEG STANCE

	Right femurs			Left femurs		
	SFN CS	IntT CS	SubT CS	SFN CS	IntT CS	SubT CS
Range	21.7-49.96	22.23-45.37	26.93-52.47	19.56-52.38	23.55-47.8	27.09- 43.04
Average	33.63	32.97	37.89	32.93	32.41	35.84

TABLE III
AVERAGE MAXIMUM VON MISES STRESS (MPA) AT THE SMALLEST FEMORAL NECK CROSS-SECTION (SFN CS), THE INTERTROCHANTERIC CROSS-SECTION (INTT CS), AND THE SUBTROCHANTERIC CROSS-SECTION (SUBT CS) OF RIGHT AND LEFT FEMURS OF 10 CLINICAL CASES DURING THE SIDEWAYS FALL

	Right femurs			Left femurs		
	SFN CS	IntT CS	SubT CS	SFN CS	IntT CS	SubT CS
Range	26.69-148.53	21.57-74.3	9.8-70.63	22.78-69.97	16.2-60.3	6.73-33.2
Average	57.22	40.74	27.08	46.52	33.48	18.66

TABLE IV
AVERAGE MAXIMUM VON MISES STRAIN AT THE SMALLEST FEMORAL NECK CROSS-SECTION (SFN CS), THE INTERTROCHANTERIC CROSS-SECTION (INTT CS), AND THE SUBTROCHANTERIC CROSS-SECTION (SUBT CS) OF RIGHT AND LEFT FEMURS OF 10 CLINICAL CASES DURING THE SINGLE-LEG STANCE

	Right femurs			Left femurs		
	SFN CS	IntT CS	SubT CS	SFN CS	IntT CS	SubT CS
Range	3.54E-03 -1.46E-02	5.89E-03 -1.74E-02	2.3E-03 - 4.75E-03	5.25E-03 - 1.55E-02	5.49E-03 - 1.87E-02	2.14E-03 - 4.34E-03
Average	9.15E-03	1.08E-02	3.32E-03	9.55E-03	1.05E-02	3.11E-03

TABLE V
AVERAGE MAXIMUM VON MISES STRAIN AT THE SMALLEST FEMORAL NECK CROSS-SECTION (SFN CS), THE INTERTROCHANTERIC CROSS-SECTION (INTT CS), AND THE SUBTROCHANTERIC CROSS-SECTION (SUBT CS) OF RIGHT AND LEFT FEMURS OF 10 CLINICAL CASES DURING THE SIDEWAYS FALL

	Right femurs			Left femurs		
	SFN CS	IntT CS	SubT CS	SFN CS	IntT CS	SubT CS
Range	1.67E-02 -1.04E-01	4.34E-02 - 1.50E-01	1.12E-03 - 6.38E-03	1.67E-02 - 7.43E-02	3.35E-02 - 1.91E-01	5.08E-04 - 3.31E-03
Average	5.29E-02	9.80E-02	2.44E-03	4.26E-02	9.37E-02	1.74E-03

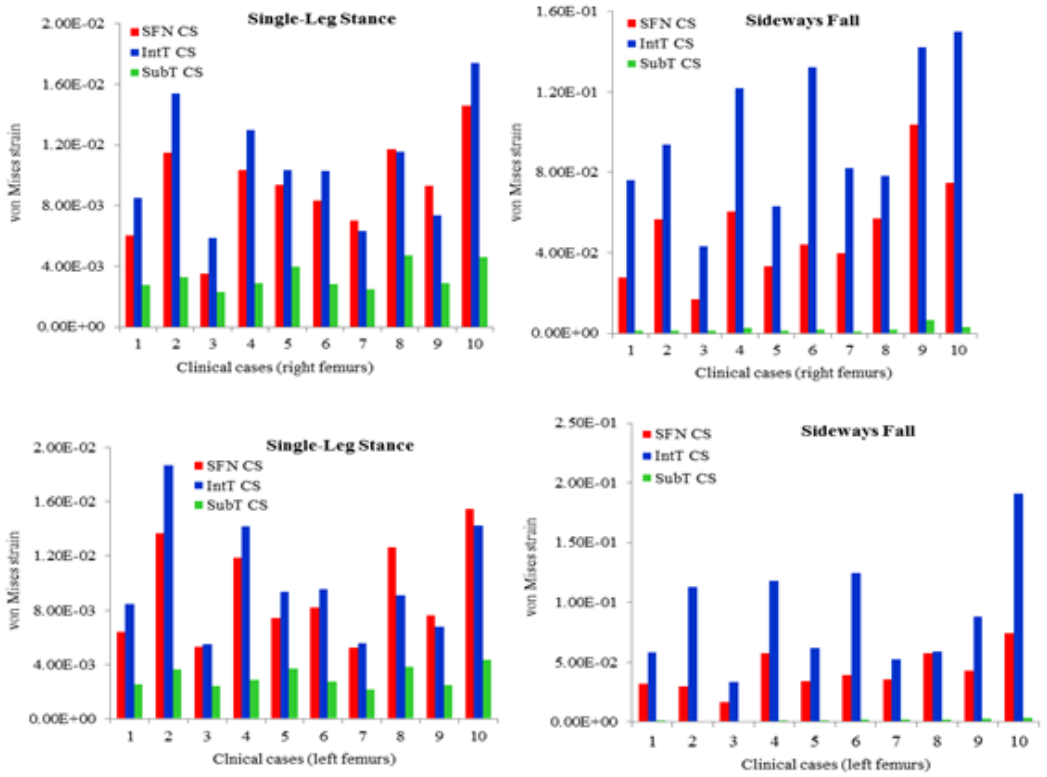

Fig. 9 The maximum von Mises strain at the smallest femoral neck cross-section (SFN CS), the intertrochanteric cross-section (IntT CS), and the subtrochanteric cross-section (SubT CS) of right and left femurs of 10 clinical cases during the single-leg stance and the sideways fall

IV. DISCUSSION

The superior femoral neck only experiences low tensile stresses during the single-leg stance (Table I and Fig. 6 (a)); according to the Wolff's law, bone in this region tends to weaken over time if alternative loading is not regularly applied. During the sideways fall, however, the same area, weakened in the normal walking, is heavily loaded in compression (Table I and Fig. 7 (b)). High compressive stress in the superior region of femoral neck during the sideways fall may initiate a fracture in this region; it propagates into the inferior aspect of the femoral neck. These results show a good agreement with the previous experimental findings [24]-[28].

However, to prevent this phenomenon during falling, femur needs to experience alternative loads within daily affairs. Therefore, physical activities are highly recommended for bone remodeling and preventing the creation of weak regions in the femur based on the Wolff's law.

The maximum von Mises stress in the femoral neck and the intertrochanteric region were larger than that in the subtrochanteric region during the sideways fall (Fig. 8 and Table III). The maximum von Mises stresses during the single-leg stance (Fig. 8 and Table II) are in the same range as those during the sideways fall (Fig. 8 and Table III). Therefore, based on the stress distribution, we should not expect significant difference between the hip fracture risk during the single-leg stance and the sideways fall, while from mechanical viewpoint, fracture risk in the sideways fall should be larger than that in the single-leg stance, as the impact force is much larger than the stance force. However, the influence of other parameters, in addition to the stress effects, should be considered to justify the larger fracture risk in the sideways fall. Bone is classified as a brittle material and the effective strains are important parameters in the failure of brittle materials, it encouraged us to investigate the effects of strains in the three critical regions of femur. Results of this study show that the maximum von Mises strains in the femoral neck and the intertrochanteric region are much higher than those in the sub trochanteric region during both the single-leg stance and the sideways fall (Fig. 9, Tables IV and V). The strains during the single-leg stance (Fig. 9 and Table IV) are much lower than those during the sideways fall (Fig. 9 and Table V), which may explain the lower hip fracture risk during the single-leg stance.

The differences between the strains in the three critical regions of femur during both the single-leg stance and the sideways fall (Fig. 9, Tables IV, and V) are much higher than the differences between the corresponding stresses (Fig. 8, Tables II, III), indicating bone failure is more sensitive to the strains because of its fragility property, so, the effects of strains should also be considered in bone fracture risk assessment. Therefore, in failure analysis of femur, an appropriate failure theory, considering both the stress and strain intensities, is needed. Strain energy criterion, which is product of both stress and strain tensors, may be an appropriate failure theory for hip fracture risk assessment and femur failure analysis based on bone failure mechanism. In our future work, strain energy criterion will be considered for hip fracture risk assessment of clinical cases.

V. Conclusion

In this study, stress and strain trends in the critical regions of femur for 10 clinical cases were identified during the single-leg stance and the sideways fall configuration. Based on the acquired stress and strain patterns; the superior region of femoral neck is highly potential location for fracture initiation during the sideways fall. It was also found that femur is more sensitive to the strain than the stress. Therefore, in failure analysis of femur, the strain effects should also be considered as well as the stress effects.

By subject-specific QCT-based finite element analysis of femur, critical regions and potential fracture locations can be recognized which it can help us in providing a proper health care planning and treatment to prevent future probable hip fractures in the elderly.

Acknowledgment

The reported research was supported by the Natural Sciences and Engineering Research Council (NSERC) of Canada, which is gratefully acknowledged.

References

[1] N. M. Resnick, and S. L. Greenspan, "'Senile' osteoporosis reconsidered," *JAMA*, vol. 261, no. 7, pp. 1025–1029,1989.
[2] M. Mirzaei, M. Keshavarzian, and V. Naeini, "Analysis of strength and failure pattern of human proximal femur using quantitative computed tomography (QCT)-based finite element method," *Bone*, vol. 64, pp. 108–114, 2014.
[3] J. H. Keyak, S. A. Rossi, K. A. Jones, C. M. Les, and H. B. Skinner, "Prediction of fracture location in the proximal femur using finite element models," *Med. Eng. Phys.*, vol. 23, no. 9, pp. 657–664, 2001.
[4] M. Bessho, I. Ohnishi, T. Matsumoto, S. Ohashi, J. Matsuyama, K. Tobita, M. Kaneko, and K. Nakamura, "Prediction of proximal femur strength using a CT-based nonlinear finite element method: Differences in predicted fracture load and site with changing load and boundary conditions," *Bone*, vol. 45, no. 2, pp. 226–231, 2009.
[5] D. Dragomir-Daescu, J. O. D. Buijs, S. McEligot, Y. Dai, R. C. Entwistle, C. Salas, L. J. M. Iii, K. E. Bennet, S. Khosla, and S. Amin, "Robust QCT/FEA Models of Proximal Femur Stiffness and Fracture Load During a Sideways Fall on the Hip," *Ann. Biomed. Eng.*, vol. 39, no. 2, pp. 742–755, 2010.
[6] J. E. M. Koivumäki, J. Thevenot, P. Pulkkinen, V. Kuhn, T. M. Link, F. Eckstein, and T. Jämsä, "Ct-based finite element models can be used to estimate experimentally measured failure loads in the proximal femur," *Bone*, vol. 50, no. 4, pp. 824–829, 2012.
[7] J. D. Michelson, A. Myers, R. Jinnah, Q. Cox, and M. Van Natta, "Epidemiology of hip fractures among the elderly. Risk factors for fracture type," *Clin. Orthop.*, vol. 311, pp. 129–135, 1995.
[8] J. H. Keyak, J. M. Meagher, H. B. Skinner, and C. D. Mote Jr, "Automated three-dimensional finite element modelling of bone: a new method," *J. Biomed. Eng.*, vol. 12, no. 5, pp. 389–397, 1990.
[9] T. M. Keaveny, R. E. Borchers, L. J. Gibson, and W. C. Hayes, "Trabecular bone modulus and strength can depend on specimen geometry," *J. Biomech.*, vol. 26, no. 8, pp. 991–1000, 1993.
[10] C. M. Les, J. H. Keyak, S. M. Stover, K. T. Taylor, and A. J. Kaneps, "Estimation of material properties in the equine metacarpus with use of quantitative computed tomography," *J. Orthop. Res. Off. Publ. Orthop. Res. Soc.*, vol. 12, no. 6, pp. 822–833, 1994.
[11] T. S. Keller, "Predicting the compressive mechanical behavior of bone," *J. Biomech.*, vol. 27, no. 9, pp. 1159–1168, 1994.
[12] J. H. Keyak, S. A. Rossi, K. A. Jones, and H. B. Skinner, "Prediction of femoral fracture load using automated finite element modeling," *J. Biomech.*, vol. 31, no. 2, pp. 125–133, 1997.
[13] D. T. Reilly, and A. H. Burstein, "The elastic and ultimate properties of compact bone tissue," *J. Biomech.*, vol. 8, no. 6, pp. 393–405, 1975.
[14] W. C. Van Buskirk, and R. B. Ashman, "The elastic moduli of bone," *Trans. American Society of Mechanical Engineers (Applied Mechanics Division), American Society of Mechanical Engineers*, New York, 1981, pp. 131–143,.
[15] T. Yoshikawa, C. h. Turner, M. Peacock, C. W. Slemenda, C. M. Weaver, D. Teegarden, P. Markwardt, and D. B. Burr, "Geometric structure of the femoral neck measured using dual-energy X-ray absorptiometry," *J. Bone Miner. Res.*, vol. 9, no. 7, pp. 1053–1064, 1994.
[16] M. Bessho, I. Ohnishi, T. Matsumoto, S. Ohashi, J. Matsuyama, K. Tobita, M. Kaneko, and K. Nakamura, "Prediction of proximal femur strength using a CT-based nonlinear finite element method: Differences in predicted fracture load and site with changing load and boundary conditions," *Bone*, vol. 45, no. 2, pp. 226–231, 2009.

[17] K. K. Nishiyama, S. Gilchrist, P. Guy, P. Cripton, and S. K. Boyd, "Proximal femur bone strength estimated by a computationally fast finite element analysis in a sideways fall configuration," *J. Biomech.*, vol. 46, no. 7, pp. 1231–1236, 2013.
[18] S. N. Robinovitch, W. C. Hayes, and T. A. McMahon, "Prediction of Femoral Impact Forces in fall on the Hip," *J. Biomech. Eng.*, vol. 113, no. 4, pp. 366–374, 1991.
[19] J. S. Kim, T. S. Park, S. B. Park, J. S. Kim, I. Y. Kim, and S. I. Kim, "Measurement of femoral neck anteversion in 3D. Part 1: 3D imaging method," *Med. Biol. Eng. Comput.*, vol. 38, no. 6, pp. 603–609, 2000.
[20] B. Atilla, A. Oznur, O. Caglar, M. Tokgozoglu, and M. Alpaslan, "Osteometry of the femora in Turkish individuals: a morphometric study in 114 cadaveric femora as an anatomic basis of femoral component design," *Acta Orthop. Traumatol. Turc.*, vol. 41, no. 1, pp. 64–68, 2007.
[21] E. Sariali, A. Mouttet, G. Pasquier, and E. Durante, "Three-Dimensional Hip Anatomy in Osteoarthritis: Analysis of the Femoral Offset," *J. Arthroplasty*, vol. 24, no. 6, pp. 990–997, 2009.
[22] R. Nikander, P. Kannus, P. Dastidar, M. Hannula, L. Harrison, T. Cervinka, N. G. Narra, R. Aktour, T. Arola, H. Eskola, S. Soimakallio, A. Heinonen, J. Hyttinen, and H. Sievänen, "Targeted exercises against hip fragility," *Osteoporos. Int.*, vol. 20, no. 8, pp. 1321–1328, 2008.
[23] B. Abrahamsen, T. van Staa, R. Ariely, M. Olson, and C. Cooper, "Excess mortality following hip fracture: a systematic epidemiological review," *Osteoporos. Int.*, vol. 20, no. 10, pp. 1633–1650, 2009.
[24] P. M. De Bakker, S. L. Manske, V. Ebacher, T. R. Oxland, P. A. Cripton, and P. Guy, "During sideways falls proximal femur fractures initiate in the superolateral cortex: Evidence from high-speed video of simulated fractures," *J. Biomech.*, vol. 42, no. 12, pp. 1917–1925, 2009.
[25] J. C. Lotz, E. J. Cheal, and W. C. Hayes, "Stress distributions within the proximal femur during gait and falls: implications for osteoporotic fracture," Osteoporos. *Int. J. Establ. Result Coop. Eur. Found. Osteoporos. Natl. Osteoporos. Found. USA*, vol. 5, no. 4, pp. 252–261, 1995.
[26] E. Verhulp, B. van Rietbergen, and R. Huiskes, "Load distribution in the healthy and osteoporotic human proximal femur during a fall to the side," *Bone*, vol. 42, no. 1, pp. 30–35, 2008.
[27] R. D. Carpenter, G. S. Beaupré, T. F. Lang, E. S. Orwoll, and D. R. Carter, "New QCT Analysis Approach Shows the Importance of Fall Orientation on Femoral Neck Strength," *J. Bone Miner. Res.*, vol. 20, no. 9, pp. 1533–1542, 2005.
[28] P. M. Mayhew, C. D. Thomas, J. G. Clement, N. Loveridge, T. J. Beck, W. Bonfield, C. J. Burgoyne, and J. Reeve, "Relation between age, femoral neck cortical stability, and hip fracture risk," *The Lancet*, vol. 366, no. 9480, pp. 129–135, 2005.